Supplemental Materials: Determination of III-V/Si absolute interface energies: impact on wetting properties

S. Pallikkara Chandrasekharan[1], I. Lucci[1], D. Gupta[1], C. Cornet[1], and L. Pedesseau[1,*]
[1]*Univ Rennes, INSA Rennes, CNRS, Institut FOTON – UMR 6082, F-35000 Rennes, France*
**Corresponding author: laurent.pedesseau@insa-rennes.fr*

I. Bulk crystals and chemical potentials

A single-point simulation for energy minimization has been computed for both Si and GaP bulk materials, leading to 0K lattice constants of 5.46Å and 5.57Å respectively. The black phosphorus and α-Ga structures were considered as extreme boundaries for the chemical potentials of P and Ga atoms in the GaP crystal leading to the so-called P-rich and Ga-rich limits.

II. Stoichiometry

The stoichiometry is an important parameter to understand the evolution of the surface, interface, or slab energies with the chemical potential (See Eq. (3) of the main article).

In order to be able to compare the effect of stoichiometry on surfaces and interfaces, a specific surface or interface stoichiometry parameter *S* is defined (Eq. (S1,S2)) as the number of P atoms minus the number of Ga atoms (Δ*N*) per unit area (lxl), normalized to the unit cell area (a_o^2).

The surface and interface stoichiometry parameters are thus given by:

$$S_{surf} = \frac{\Delta N_{surf}}{\left(\frac{A}{a_o^2}\right)} \quad \text{(S1)}$$

$$S_{int} = \frac{\Delta N_{slab} - \sum_{j=Y,Z}(\Delta N_{surf}^{j})}{\left(\frac{A}{a_o^2}\right)} = \frac{\Delta N_{int}}{\left(\frac{A}{a_o^2}\right)} \quad \text{(S2)}$$

where ΔN_{surf}, ΔN_{slab}, and ΔN_{surf}^{j} are respectively the stoichiometries of the studied surface, of the slab, and ofthe surfaces *Y* and *Z* (the top and bottom specific surfaces used for interface energy calculations). *A* is the in-plane surface area of the surfaces or slabs.

The S parameter gives an idea about the excess or lack of charge as compared to an ideal case where the charges are compensated. To be more explicit, in general, the lower the *S* parameter, the more stable the configuration. One ideal case is when the *S* parameter equals to zero. In this case, the surface or interface becomes stoichiometric and respects the electron counting model (ECM) criteria [1]. This provides an argument to explain the good stability [1] of charge-compensated surfaces or interfaces.

III. Computational details

For DFT calculations, $1s^{0.75}$, $1s^{1.25}$, $3s^2 3p^3$, and $4s^2 3d^{10} 4p^1$ were used as valence electrons for the fictitious H*(P) with a net charge of 0.75e to compensate P, and the fictitious H*(Ga) with a net charge of 1.25e to compensate Ga. The two fictitious H*, Ga and P atoms have been built with ATOM code; the pseudopotential generation distributed as part of the SIESTA software package.

IV. H*-passivation methodology

For convenience, we use the term "H*-passivation methodology" for "localized basis sets including H*-passivation methodology". In the following, we i) show the interest of the H*-passivation methodology, ii) test the methodology on a non-polar surface, and iii) apply the methodology to a polar surface.

A. Interest of the H*-passivation methodology

This methodology is useful mainly for three reasons. First, one can passivate a surface to mimic the bulk of a III-V semiconductor. Second, it is possible to reduce the impact of the surface dipole which has been studied by G. Makov and C. Payne in their pioneering work [2]. Finally, by coupling this H*-passivation to a localized basis sets code such as SIESTA, one can really reach the convergence of the Electric dipole and also total energy for a polar slab with a tiny contribution of the coulombic part, and surface dipole due to the images of the slab [2]. To really understand this issue, two studies are proposed hereafter. The first one, a 0D case, shows a water molecule with its dipole in a periodic box, and gives the calculated Energy *E(L)* and Electric dipole *p(L)* as a function of the size of the box *L*. Figure S1 shows the Electric dipole *p(L)* of a water molecule in a periodic box condition as a function of the vacuum thickness. The DFT PBE numerical simulation is fitted with three terms namely p_o, $p_{(d—d)}$ and $p_{(d\text{-}ind—d)}$. Indeed, p_o is the Electric dipole when *L* tends toward infinity. So, an extrapolation can be made to get this value. The two other terms are the Electric dipoles due to dipole-dipole interaction and (dipole induced)-dipole interaction. The strongest term is the dipole-dipole interaction which decays as L^{-3} as compared to the (dipole induced)-dipole interaction which decays as L^{-6}. For a water molecule the $p_{(d—d)}$ term starts to vanish for *L* larger than 12 Å, indicating in

this case, that one can easily consider a vacuum thickness > 12 Å to get rid of parasitic dipole contributions. For the second example, we choose a more complex situation with a polar slab through the direction (111)A and Ga Trimers on top of one side and passivated on the other side. The passivated side of the slab is mandatory to mimic the bulk on the bottom of the slab and reduce these effects on the total Electric dipole. Here we have a 2D case. The Figure S2 shows the Electric dipole *p(L)* of the slab GaP(111)A Ga-Trimer as a function of the vacuum thickness *L*. Here the behavior is quite different. There are two terms which are non-negligible for *L* lower than 50Å which are the dipole-dipole interaction $p_{(d-d)}$ and the Coulombic interaction. When the vacuum thickness *L* is larger than 50 Å, the dominant term is the Coulombic contribution. This term starts to vanish around 450 Å and we choose this value for the rest of this study. However, to get this Coulombic interaction definitively disappears it is needed to go up to 10000Å.

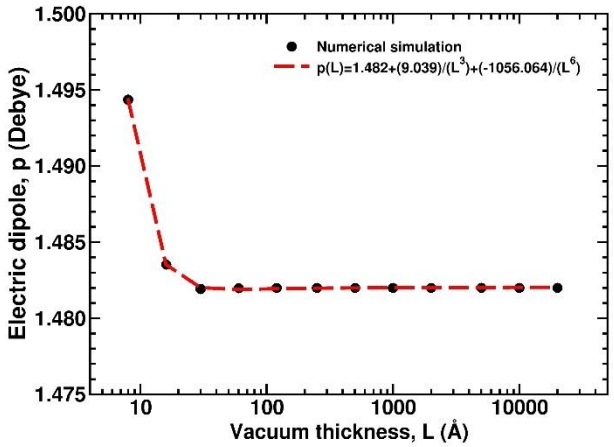

FIG. S1: Electric dipole *p(L)*, in Debye, of a water molecule in a box as a function of the vacuum thickness, *L* in Å.

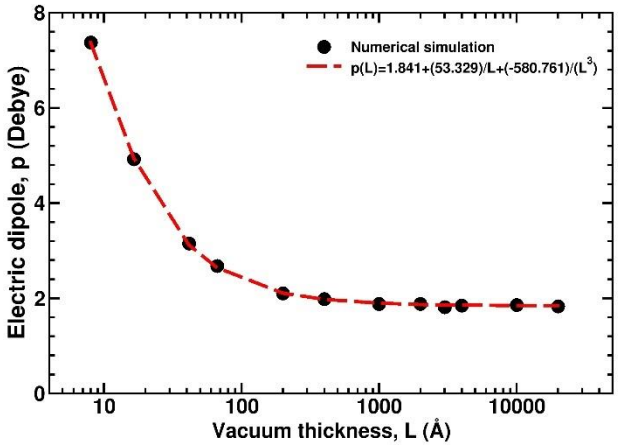

FIG. S2: Electric dipole *p(L)*, in Debye, of the slab GaP(111)A Ga-Trimer as a function of the vacuum thickness *L*, in Å.

In practice, a plane wave code will barely reach 20 Å of vacuum thickness. On the contrary, a localized basis sets (here SIESTA) code can go up to 20 thousand Å without any difficulties.

This is why a localized basis sets (here SIESTA) including the H*-passivation is the strategy that we adopt for the rest of the study. In the following, the validity of the approach is considered, by applying it on non-polar surfaces.

B. Testing the methodology on non-polar surfaces

In order to check the validity of the localized basis sets including H*-passivation methodology, we compare in the following two different methods: i) the H*-passivation approach and ii) the one used for the non-polar surface (see the main article file) on a simple non-polar P-rich GaP(001) (2x1) reconstruction (this surface is usually not considered as the most stable one as it does not fulfill the ECM criterion). The general strategy of the H*-passivation approach, is to passivate the bottom surface with fictitious hydrogen atoms, whose chemical potentials are known (See. Fig. S3 (b)), and thus determine the top surface energy.

In the case of H*-passivation approach, the surface energy equation is therefore modified with respect to the symmetric case, by including a new term coming from the fictitious H* atoms:

$$\gamma_{polar-GaP} = \frac{E_{slab} - N_{Ga}\mu_{GaP}^{GaP-bulk} - (N_P - N_{Ga})\mu_P - N_{H^*}^P \mu_{H^*}^P}{A} \qquad \text{(S3)}$$

where E_{slab} is the total energy of the slab with one side H*-passivated, $N_{H^*}^P$ the number of fictitious hydrogens bonded to the P atoms of the bottom surface and $\mu_{H^*}^P$ is their chemical potential.

The difficulty of this calculation is to determine the fictitious H* chemical potential $\mu_{H^*}^P$. Indeed, to do this, we first computed the total energy of the P-rich GaP(001)(2x1) slab with both-surfaces passivated by fictitious hydrogens H* (Fig. S3(a)). To this aim, all the Ga and P atoms were kept frozen in the bulk position while only the fictitious H* atoms were allowed to relax. Then, we applied the following equation to determine $\mu_{H^*}^P$:

$$\mu_{H^*}^P = \frac{E_{slab}^{H^*-passivated} - N_{Ga}\mu_{GaP}^{GaP-bulk} - (N_P - N_{Ga})\mu_P}{N_{H^*}} \qquad \text{(S4)}$$

where $E_{slab}^{H^*-passivated}$ is the total energy of the slab passivated on both sides. The both-side passivated slab in Fig. S3(a) is non-stoichiometric, i.e., $N_P \neq N_{Ga}$. That is why the $\mu_{H^*}^P$ must be expressed as a function of the phosphorus chemical potential.

After that, we built a slab having only the bottom surface passivated by the fictitious-H* kept in their positions of

minimum energy. The top surface was allowed to relax in its P-rich GaP(001) (2x1) reconstruction (see slab in Fig. S3(b)). In particular, the top surface in addition to the subsurface (about 6Å) was allowed to relax into its minimum energy and all the other atoms were kept frozen in the bulk position. By applying in Eq. (S3) the $\mu_{H^*}^P$ found through Eq. (S4), we finally determined the P-rich GaP(001) (2x1) surface energy which differs just by 0.49 meV/Å² from the one determined in the symmetric case (see Table SI), that confirms the validity of the approach.

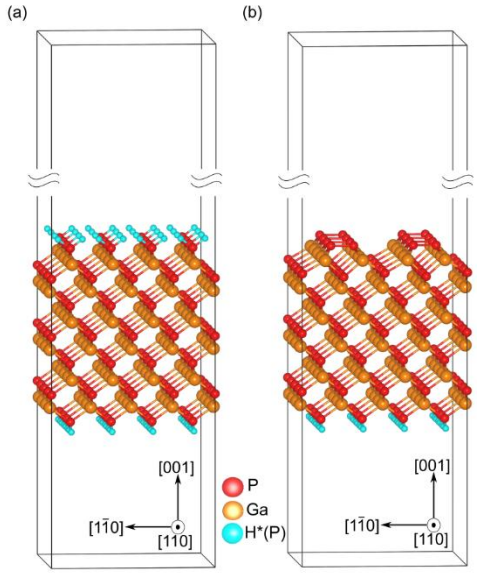

FIG. S3: Slab built for determining: (a) the fictitious H* chemical potential, and (b) the P-rich (2x1) surface energy using the H*-passivated surface on the bottom.

Table SI. Surface energies comparison between P-rich GaP(001) (2x1) without and with H*-passivation strategies.

DFT strategy	N_{Ga}	N_P	Energy (meV/Å²)	
			P-rich	Ga-rich
Symmetric	96	112	57.19	87.10
H*-passivated	96	112	57.68	87.59

C. Applying the methodology on polar surfaces

This H*-passivation strategy is then used to determine the surface energies of the stable polar GaP(1 1 4), GaP(2 5 11), and GaP(1 1 1) surfaces. The stability of (1 1 4) surfaces for III-V semiconductors has been studied in many previous works. Especially, experimental evidences supported by DFT calculations were reported for GaAs(114) [3] or InAs(114) [4]. The stability of GaP(114) facets was also discussed recently [5]. Here, we apply the H*-passivation strategy for the determination of GaP(114) surface energies. For the polar GaP(114) surfaces which have a thickness of about 25Å, the Ga-rich GaP(114)A-α2(2x1) and the P-rich GaP(114)B-α2(2x1) surfaces were passivated by the fictitious H^* with fractionally charged hydrogen (1.25e and 0.75e) for Ga and P dangling bonds. The slabs used for the calculations and the surface atomic structure are given in Fig. S4.

To determine the surface energies, we use the same procedure than the one previously described, except that hydrogen atoms are now bonded to both Ga and P atoms. The chemical potential of these fictitious hydrogens has thus to be treated independently and the surface energy is now given by:

$$\gamma_{polar} = \frac{\frac{E_{slab} - N_{Ga}\mu_{GaP}^{GaP-bulk} - (N_P - N_{Ga})\mu_P}{A}}{\frac{-N_{H^*}^{Ga}\mu_{H^*}^{Ga} - N_{H^*}^{P}\mu_{H^*}^{P}}{A}} \quad \text{(S5)}$$

where E_{slab} is the total energy of the slab with one side H*-passivated, $N_{H^*}^P$ and $N_{H^*}^{Ga}$ the number of fictitious hydrogens bonded to the P or Ga atoms of the bottom surface and $\mu_{H^*}^P$, $\mu_{H^*}^{Ga}$ are their respective chemical potential.

In order to strengthen the validation of the H*-passivation method in the case of GaP(114) surface, we also calculated the surface energy for the polar GaAs(114) as a test to compare with previous studies [3]. As a result, we found exactly the same surface energy (53.0 meV/Å²) for the Ga-rich GaAs(114)A-α2(2x1) reconstruction. Moreover, the value for the P-rich GaAs(114)B-α2(2x1) surface energy has also been estimated at 59.1 meV/Å².

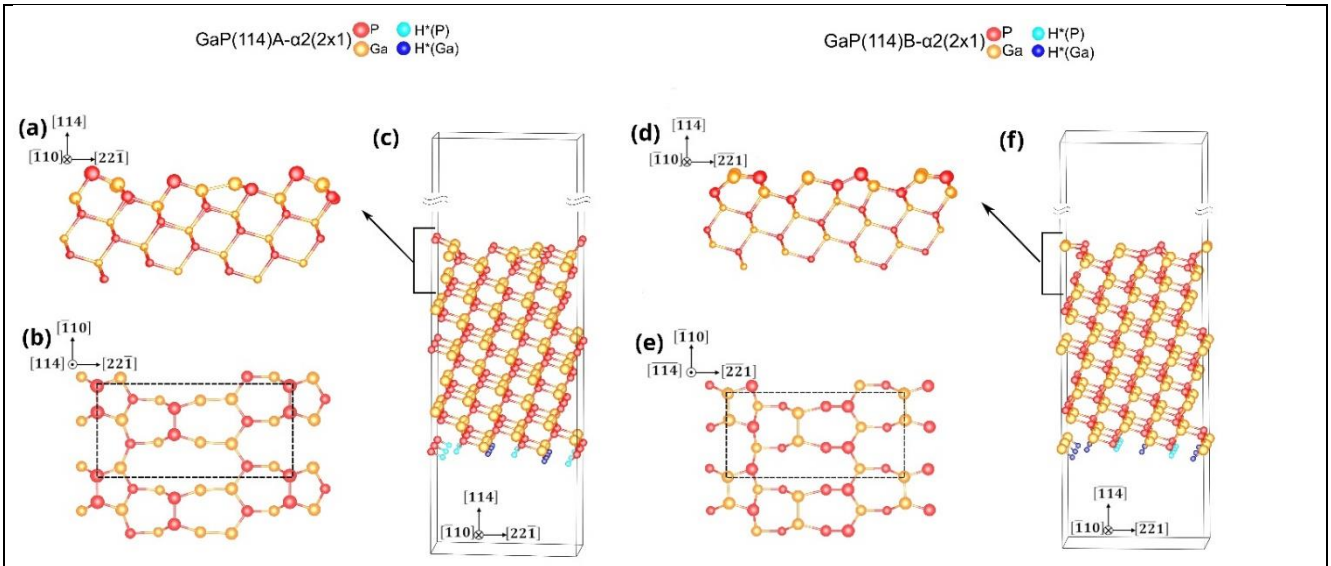

FIG. S4: (a) Side profile, (b) top view, and (c) the slab realized for GaP(114)A-α2(1x1) surface. (d) Side profile, (e) top view and (f) the slab realized for GaP(114)B-α2(1x1) surface. The top view is over {114}, {$\bar{1}$10} and {22$\bar{1}$} axis. The surface investigated is on top and the bottom surface is H*-passivated. Dashed lines in the top views indicate the unit cells of the reconstructions.

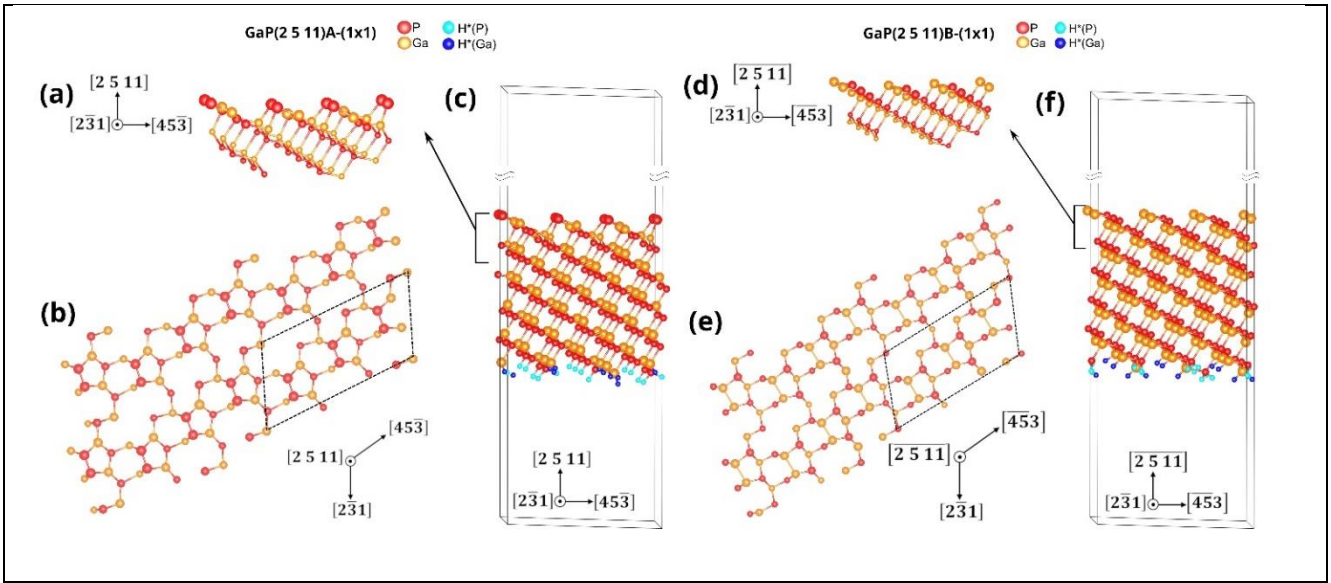

FIG. S5: (a) Side profile, (b) top view, and (c) the slab realized for GaP(2 5 11)A-(1x1) surface. (d) Side profile, (e) top view and (f) the slab realized for GaP(2 5 11)B-(1x1) surface. The top view is over {2 5 11}, {2$\bar{3}$1} and {45$\bar{3}$} axis. The surface investigated is on top and the bottom surface is H*-passivated. Dashed lines in the top views indicate the unit cells of the reconstructions.

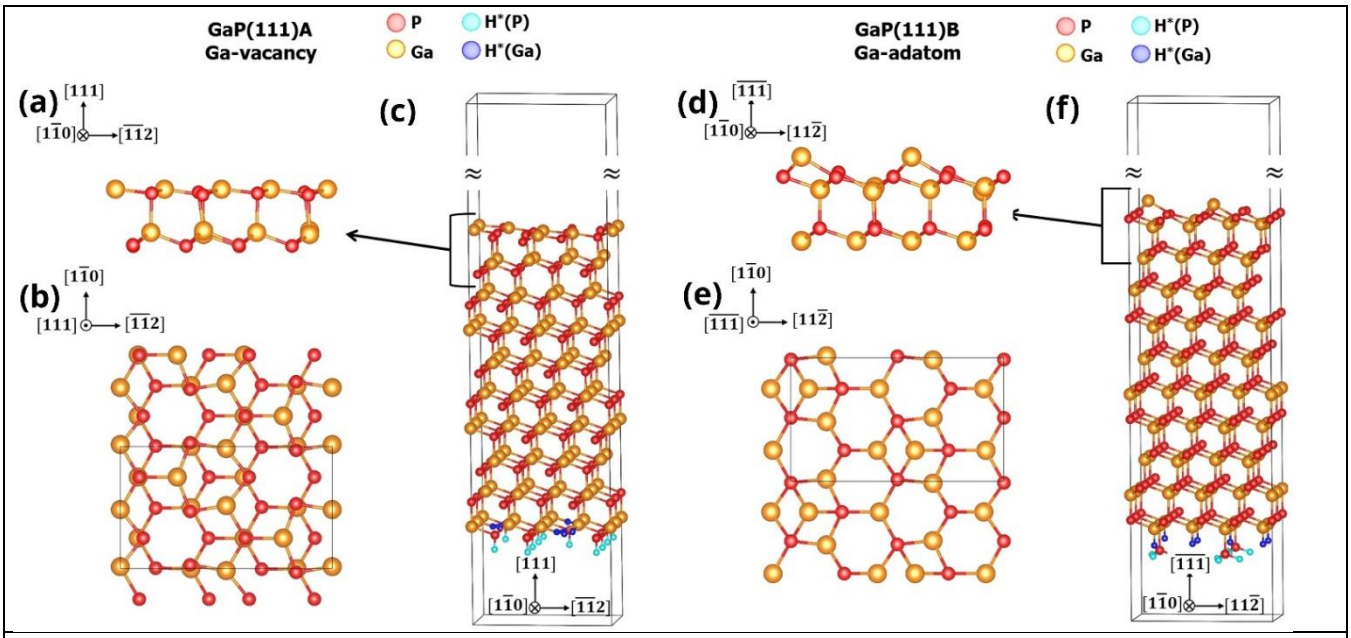

FIG. S6: (a) Side profile, (b) top view, and (c) the slab realized for GaP(111)A Ga-vacancy surface. (d) Side profile, (e) top view and (f) the slab realized for GaP(111)B Ga-adatom surface. The top view is over {111}, {1$\bar{1}$0} and {$\bar{1}\bar{1}$2} axis. The surface investigated is on top and the bottom surface is H*-passivated. Dashed lines in the top views indicate the unit cells of the reconstructions.

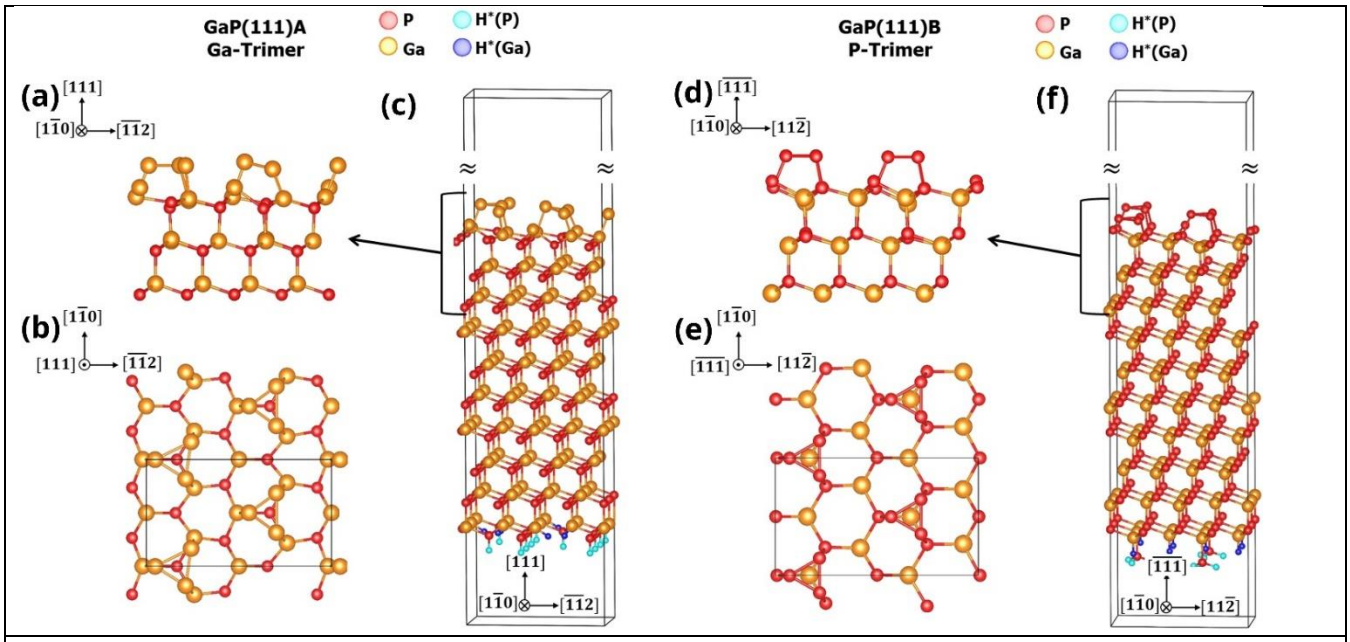

FIG. S7: (a) Side profile, (b) top view, and (c) the slab realized for GaP(111)A Ga-Trimer surface. (d) Side profile, (e) top view and (f) the slab realized for GaP(111)B P-Trimer surface. The top view is over {111}, {1$\bar{1}$0} and {$\bar{1}\bar{1}$2} axis. The surface investigated is on top and the bottom surface is H*-passivated. Dashed lines in the top views indicate the unit cells of the reconstructions.

V. The phase diagram of GaSiP

We calculated the phase stability diagram for the GaSiP material system, based on the formation energies of all materials and secondary phases with GGA functional. [6,7].

The possible secondary phases that were identified in the system are: SiP, SiP_2, $GaSiP_3$, $GaSi_3$, GaSi, and Ga_3Si. The calculated formation energies for these compounds are reported in Table SII. In addition, the phase stability diagram of GaSiP compounds is given in Fig. S8, and the zoom on the GaP/Si stability region is given in Fig. S9. The blue shaded area of the stability diagram is the region of chemical potential where only GaP and Si phases can form. Thus, in this diagram, we show that, except for extreme Ga-poor and Si-rich growth conditions, the formation of the GaP/Si interface will be energetically preferred over the formation of all other secondary phases.

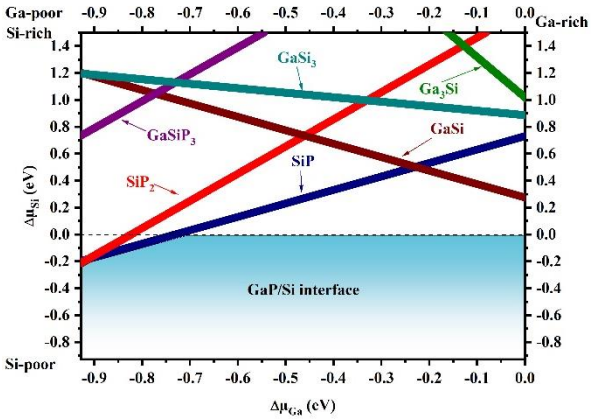

FIG. S8: GaP/Si interface phase diagram with varying chemical potentials. The stable potential region in the shaded area is where the GaP/Si interface can occur without interference from secondary phases.

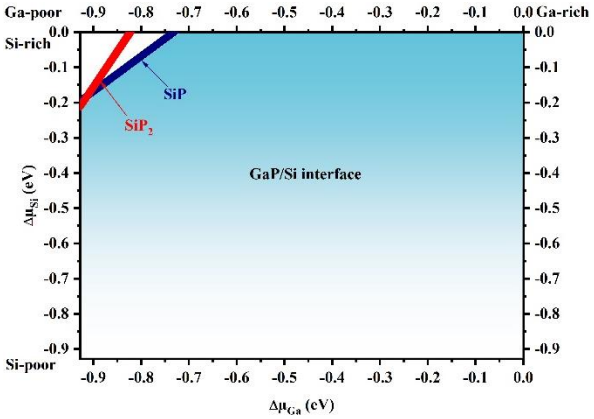

FIG. S9: Zoom on GaP/Si interface phase diagram with varying chemical potentials. The stable potential region in the shaded area is where the GaP/Si interface can occur without interference from secondary phases.

Table SII. The DFT (GGA functional) calculated heat formation energies (ΔH_f) of phases in the region of GaP/Si interface.

Compound	$\Delta H_f(eV)$
Si	0
SiP	-0.196
SiP_2	-0.211
GaSi	0.274
$GaSi_3$	2.658
Ga_3Si	1.019
$GaSiP_3$	-0.192
GaP	-0.928

[1] M. D. Pashley, *Electron Counting Model and Its Application to Island Structures on Molecular-Beam Epitaxy Grown GaAs(001) and ZnSe(001)*, Phys. Rev. B **40**, 10481 (1989).

[2] G. Makov and M. C. Payne, *Periodic Boundary Conditions in Ab Initio Calculations*, Phys. Rev. B **51**, 4014 (1995).

[3] J. Márquez, P. Kratzer, L. Geelhaar, K. Jacobi, and M. Scheffler, *Atomic Structure of the Stoichiometric GaAs(114) Surface*, Phys. Rev. Lett. **86**, 115 (2001).

[4] A. Ponchet, L. Pedesseau, A. Le Corre, C. Cornet, and N. Bertru, *Shape Transition in InAs Nanostructures Formed by Stranski-Krastanow Growth Mode on InP (001) Substrate*, Appl. Phys. Lett. **114**, 173102 (2019).

[5] I. Lucci et al., *A Stress-Free and Textured GaP Template on Silicon for Solar Water Splitting*, Adv. Funct. Mater. **28**, 1801585 (2018).

[6] S. Lany, *Semiconductor Thermochemistry in Density Functional Calculations*, Phys. Rev. B **78**, 245207 (2008).

[7] V. Stevanović, S. Lany, X. Zhang, and A. Zunger, *Correcting Density Functional Theory for Accurate Predictions of Compound Enthalpies of Formation: Fitted Elemental-Phase Reference Energies*, Phys. Rev. B **85**, 115104 (2012).